Praise Worthy Prize
International Review of Electrical Engineering (I.R.E.E.), Vol. 11, N. 6
ISSN 1827- 6660 November – December 2016

Three-Phase Magnetic Field Tested in Wireless Power Transfer System

L. F. Romba[1], Stanimir S. Valtchev[1], R. Melício[2, 3]

Abstract – *This paper presents a magnetic field three dimensional mapping produced by a three-phase prototype for wireless power transfer. The presented magnetic field mapping is a contribution to improve the design of electric vehicles battery chargers using the wireless power transfer. To collect the magnetic field data, a prototype was built, in order to support the tests. The prototype primary is an electrical three-phase system that allows to be connected electrically and geometrically in star or delta. The losses due to the magnetic field dispersion and the generated interferences in the surrounding equipment or in human body are discussed. The different standards organizations related to electric vehicles battery chargers are presented. Finally the magnetic field influence on the human body is addressed.*

Keywords: *Electromagnetic Compatibility, Wireless Power Transfer, Battery Chargers, Magnetic Field*

Nomenclature

B	Magnetic field intensity
d	Distance from the conductor center
D	Distance between a generic point over the coil axis and the coil edge
E	Electromotive force
EF	Electric field
dl	Incremental length
dS	Incremental surface
G	Antenna gain
H	Magnetic field strength
I	Electric current
J	Current density
k_{TR}	Coupling coefficient
L_R	Receiver coil inductance
L_T	Transmitter coil inductance
M	Mutual inductance
MF	Magnetic field
n	Number of turns per meter
P	Maximum output power
PD	Power density
r	Conductor radius
R	Coil radius
σ	Electrical conductivity
Φ	Total magnetic flux
Φ_B	Magnetic flux
μ	Magnetic permeability
μ_0	Vacuum permeability
CEN	European Committee for Standardization
CENELEC	European Committee for Electrotechnical Standardization
EMC	Electromagnetic compatibility
ETSI	European Telecommunications Standards Institute
EV	Electric vehicle
IEC	International Electrotechnical Commission.
IPT	Inductive power transfer
IPQ	Portuguese Quality Institute
ISA	International Federation of National Standardizing Associations
ISO	International Organization for Standardization
MCR	Magnetically coupled resonator
RF	Radio frequency
SC	Subcommittees
TC	Technical committee
UNSCC	United Nations Standards Coordinating Committee
WG	Working group
WPT	Wireless power transfer

I. Introduction

The idea of transmitting electrical energy through the air was an old dream of Nikola Tesla [1]. The history of the WPT systems began in 1891 when Tesla invented his famous Tesla coil [2]. A generic WPT can be regarded as an efficient method of power transmission from one point to another through the air or the vacuum without the use of electrical cables or other conductive substance [3], [4]. The WPT can be applied in an instantaneous energy consumption, namely peak consumption or continuous energy delivery but where the connection cables are inconvenient, expensive, dangerous or impossible to use [4], [5]. The technologies used in the wireless power transfer systems can be categorized, according to functions of distance at which they can perform the power transmission efficiently, i.e. short

 DOI: 10.15866/iree.v11i6.9889

range, middle range and long range [6], [7].

The distance covered by the term “short range” starts from a few millimeters or centimeters. The middle range covers distances from a few centimeters to several meters and it may involve the use of repeaters. These two are also named “near field” technologies. Finally, the long range covers distances of meters up to many kilometers [6], [7]. The term used here is “far field”.

The first two categories of the WPT technology are nonradiative, i.e., the carrier field is either magnetic or electric, but not electromagnetic (radio transmission).

The far field is radiative, because is based on electromagnetic emission [7], [8]. The latest advances in semiconductor technology and magnetic materials helped the development of more efficient wireless power transfer in the near field technology [9]. The WPT is mostly a near field technology. It is still not available as an alternative to the power transmission by wire.

The wire line system was established in the second half of the 19th century as the only electric grid, while Heinrich Hertz and Nikola Tesla had taken the first steps to the dream of wireless electric transmission [10] in the late 19th century. The recent history of the WPT restarted mainly in the "far field" technology, i.e. by microwaves (Microwaves Power Transmission). In the 1960s, William C. Brawn studied and experimented WPT based on telecommunications and radar technologies achievements in the World War II [10]. He developed a special antenna block called "rectenna" for receiving and rectifying the microwaves [11]-[16].

A developed concept proposed later by Peter Glaser was to place power satellites constellation in geostationary equatorial orbit sending the energy obtained in space, to the ground station. The near field WPT is the most widely used now, e.g. in implantable biomedical devices. The main advantage of these implants lies in the reduced risk of postoperative infections and patient discomfort [17]-[21].

The technology that applies near field and inductive coupling is called IPT. Additionally this system is also being used to charge batteries for consumer electronic devices and more recently, it is also proposed to charge the batteries of EV, both hybrid and pure electric vehicles. In this transfer method the best efficiency and power is achieved by magnetic field. The principle is similar to the transformer, having resonant loops in the primary and secondary, tuned at the same frequency. The resonance can be tuned by connecting capacitors in series or in parallel on each side [22]. One of the many issues associated with the IPT is the adaptive matching method.

During the operation, the load impedance varies with the distance and alignment between the primary and secondary circuits, and the impedance matching is necessary for achieving efficient power transfer. One of the methods consists in working at fixed frequency. It is easy to be implemented but it has serious limitations when the air gap and/or impedances change significantly.

The second method, working by tracked the emitted frequency, could be implemented by controlling the resonance in the primary, or the secondary side, or in the both sides [23], [24].

The Magnetic Coupling Resonance used for the mid-range distance is similar to the short-range technology.

However, the tuning circuits are physically separated and, working close to the transmitter/receiver circuits.

These wireless power systems MCR, can achieve high efficiency than the IPS over a larger distance by their high quality factor and maintained same resonant frequency [23], [24]. The wireless power transfer is essential for the spread of EV as it provides a safe and convenient charging of the cars batteries. To achieve wireless charging, the WPT system must satisfy three conditions: high efficiency, large air gaps and high power. The WPT, especially when the strong magnetic resonance is applied, satisfies these three conditions. The three phase wireless transmission permits a higher energy transfer, and is less critical to the misalignment [24].

I.1. The Standards Organizations

The equipment manufactured by electrical and electronic components must comply with the rules and standards, mainly to protect the users. This protection covers areas such as the use of reduced voltages in control systems to the influence of the electromagnetic field on the human body. Some world entities that have responsibility for study, approval and publisher the international rules and standards are as following:

The IEC [25] had its beginnings in the Resolution of the Chamber of Government Delegates in September 1904, in the International Electrical Congress in St. Louis, USA. As in the other Electrotechnical organizations, the main objective is to prepare and publish the International Standards with regard to electric and electronic technologies. The structure of this Organization is based on TC, SC and WG. The TC and the SC prepare all the technical documentation for each specific sector and submits the documents to the members of the IEC for vote. Each National Committee represents the industry, the academia, the regulators and the consumers from the corresponding country.

The IEC defines the EMC as: "… EMC describes the ability of electronic and electrical systems or components to work correctly when they are close together. In practice, this means that the electromagnetic disturbances from each part of equipment must be limited and also each item must have an adequate level of immunity to the disturbances in its environment…".

The ISA, founded in 1926, was the beginning of the ISO [26]. Only after the World War II, it was made one approach to the UNSCC in order to create a new global organization to coordinate all activities relating to studies and publisher the new standards. The new organization ISO was born in 1946 in London, when at a meeting of delegates of the twenty-five countries such were deliberated. The European Commission recognized through EU Regulation 1025/2012/EC three European entities that make part of this organization. The three

entities are: the CEN, the CENELEC and the ETSI.

These three entities are part of the European Standardization Organizations and all of then have the responsibility of to study, to elaborate and the publication of the standards for the EU. The CEN and the CENELEC have strong connections with the ISO and IEC respectively through the National Standards Bodies. As an example, the TC responsible for electric road vehicles in the CEN organization is the TC 301 [27].

I.2. The Electric Vehicle Standardization Responsibility

As an example of some contradictions among organizations about the same standards, it can be indicated the following:

For the EVs and the HEVs, being road vehicles, the responsibility in ISO is the TC 22/SC 21 and this subcommittee has three WGs. However, for the IEC, these vehicles are considered electric devices, ruled by competences attributed to the TC 69 with two WGs [28].

In order to reconcile the divergences that have been manifested in the past between the two TCs (ISO TC22/SC21 and IEC TC 69), some collaboration have been tried since a long time. A consensus agreement was established in 1996, defining the competencies of the respective committees. More recently, a Memorandum of

Understanding between ISO and IEC was signed, valid for all types of road vehicles and its equipment, clarifying the collaboration rules and ways of working [28]. There are substantial differences between regulations and standards. The standards are developed by the technical community and are voluntary adopted, while regulations are governmentally endorsed documents, enforceable as laws [28].

II. Modeling

The power density *PD* is a function of the electric field *EF* and the magnetic field *MF*. Hence, for any transmitter, the *PD* in (W/m^2) [29], [30], [34]-[36] is given by:

$$PD = \frac{PG}{4\pi d^2} \tag{1}$$

The *EF* is associated with the presence of electric charges, while the magnetic field associated with the physical movement of electric charges. The *MF* can be specified through the *B* or through the *H*.

The magnetic field and the magnetic field strength are associated given by:

$$B = \mu H \tag{2}$$

The human body's internal current and the energy absorbed by the tissues depend on the coupling mechanisms and frequency of electromagnetic field that pass through the body. The internal electric field and the current density are expressed by Ohm Law given by:

$$J = \sigma\ E \tag{3}$$

Considering the standards *J* is in the range up to 10 MHz. The models for the study of the magnetic field influence on the human body, assume that the body has homogeneous and isotropic conductivity.

Simple models are applied, consisting of circular loops, to estimate the induced currents in various organs or regions of the body. Having in mind the Faraday Law of induction, for a pure sinusoidal waveform of the field, at a frequency *f* is given by:

$$J = \pi R f \sigma B \tag{4}$$

when a current flows through a conductor, a magnetic field is generated. The frequency of this magnetic field is the same as that of the current that provoked it.

If a second conductor is nearby, an induced *E* will be created as stated by Faraday Law given by:

$$E = -\frac{\partial \Phi_B}{\partial t} \tag{5}$$

The *B* in non-magnetic environment, considering a generic closed path around a conductor with an incremental length *dl* and with the same direction as the magnetic field, is a function of the current through the conductor given by:

$$\int B\,dl = i\mu_0 \tag{6}$$

Considering (6), since the path of *B* around a straight conductor is always cylindrical, then at the distance from the conductor center *d* is given by:

$$\int Bdl = B\,2\pi\,d \tag{7}$$

As the magnetic field strength is inversely proportional to the distance the distance from the conductor center, then *B* is given by:

$$B = \frac{\mu_0}{2\,\pi\,d} i \tag{8}$$

The total flux Φ is given by:

$$\Phi = \oint \vec{B}\,\vec{dS} \tag{9}$$

Considering the Ampere Law the strength of the magnetic induction is given by:

$$\Phi = \oint \vec{B}\,\vec{dS} = \mu_0\ I_{enclosed} \tag{10}$$

Considering a coil *B* is given by:

$$B = \mu_0\ I\ n \tag{11}$$

For locations along the coil axis, it should be considered that the $\overrightarrow{dB}$ is produced inside one turn.

The integral of complete coil should be taken, to find $\vec{B}$. A coil of radius R carries a current I and creates a magnetic induction due to a tiny segment of the coil given by:

$$\overrightarrow{dB} = \frac{I\mu_0}{4\pi}\frac{\overrightarrow{dS}\,r}{R^2} \tag{12}$$

Considering that the vertical components are canceled $dB_{horizontal}$ is given by:

$$dB_{horizontal} = \frac{I\mu_0}{4\pi}\frac{dS}{D^2+R^2}\frac{R}{\left(D^2+R^2\right)^{1/2}} \tag{13}$$

The total magnetic induction is given by:

$$\vec{B} = \frac{I\mu_0}{4\pi}\frac{R}{\left(D^2+R^2\right)^{3/2}}\int dS \tag{14}$$

The L_T and L_R, are mutually coupled. The M as a function of the k_{TR} given by:

$$M = k_{TR}(L_T L_R)^{1/2} \tag{15}$$

The k_{TR} is a non-dimensional quantity having values between 0 and 1.

III. Experimental Part

The study presented in this paper was performed in the Laboratory of Power Electronics, Faculty of Science and Technology, New University of Lisbon, Portugal.

The prototype was created by three coils connected in star and delta, separately, to form a three phase system supplied by 50 Hz frequency [31]-[33]. It appears that the behavior of the three phase magnetic induction measured on this prototype as base of WPT system. The vacuum permeability value is $\mu_0 = 4\,\pi 10^{-7}$ H/m .

The primary coils are wound on magnetic cores shaped in parallelepiped form. Each coil has 110 turns, assembled in two layers. The core coils are equal and have the following dimensions: length 180 mm, height 300 mm and thickness 60 mm. The primary coils are identified by colours: red, yellow and white as shown in Fig. 2 and Fig. 3.

The probe coil, i.e. the secondary, is assembled on a cylindrical core shape of laminated ferromagnetic material and has 180 turns. This core has the following dimensions: length 130 mm and diameter 28 mm.

The electrical characteristics of this coil are the following: inductance value of 3,56 mH and the resistance value of 0,7 Ω.

The platform shown in Fig. 1 is built of non-ferromagnetic material, namely K-line, with the following dimensions: length 1000 mm and width 700 mm. The tests were performed on this platform.

The two geometric configurations, delta and star, are shown in Fig. 2 and Fig. 3. Two sets of lines are drawn on the platform surface. The first set of lines are centred ones, the second set are radial lines. These radial lines are drawn at angles of 30° between each other. On each of radial lines, are marked distances of 100 mm, 200 mm and 300 mm. On this prototype, a significant set of tests was performed, that enables the mapping of the magnetic induction, in X, Y and Z coordinates. The total covered surface value is 28,27 dm^2. Table I summarizes the measured parameters of the primary windings.

Table II summarizes the inductive reactance and the impedance calculated for the primary windings.

Fig. 1. The platform built in Kline material

Fig. 2. Prototype built. The primary coils in delta geometric configuration

Fig. 3. The primary coils in star geometric configuration

TABLE I
DATA MEASURED FOR THE PRIMARY WINDINGS

Coil	Inductance (mH)	Resistance (Ω)
Red	8,6	1,7
Yellow	8,66	1,6
White	9,43	1,6

The tests were performed by applying, in sequence, a RMS voltage value of 20 V and 30 V at the coils that form the primary circuit.

At each test point the values were obtained by the probe in three positions, vertical, horizontal longitudinal and horizontal transversal, as shown in Fig. 4, Fig. 5 and Fig. 6, at the three circumferences, with radio value of 100 mm, 200 mm and 300 mm.

Table III and Table IV summarize the currents in each primary coil for the input RMS voltage value of 20 V and of 30 V. They are applied by a three-phase variable transformer in star and delta electrical configurations.

TABLE II
PRIMARY, INDUCTIVE REACTANCE AND IMPEDANCE

Coil	Inductive reactance (Ω)	Impedance (Ω)
Red	2,7	3,19
Yellow	2,72	3,16
White	2,96	3,37

TABLE III
CURRENT IN EACH PRIMARY COIL IN STAR ELECTRICAL CONFIGURATION

	20 V	30 V
Coil	Current (A)	Current (A)
Red	6,3	9,4
Yellow	6,3	9,5
White	5,9	8,9

TABLE IV
CURRENT IN EACH PRIMARY COIL IN DELTA ELECTRICAL CONFIGURATION

	20 V	30 V
Coil	Current (A)	Current (A)
Red	10,8	16,3
Yellow	10,9	16,5
White	10,3	15,4

Fig. 4. Probe in vertical position

Fig. 5. Probe in horizontal longitudinal position

Fig. 6. Probe in horizontal transversal position

IV. Case Study

The results shown in this case study are divided in two sections IV.1 and IV.2. The section IV.1 (Fig. 7 to Fig. 17) shows the magnetic induction values measured when the primary coils are electrically connected in delta, but in star geometric configuration. The section IV.2 (Fig. 18 to Fig. 29) shows the magnetic induction values measured when the electrical configuration is maintained but the coils are in delta geometric configuration.

The average electric current value through each coil is 16,07 A (Table III, column 30 V).

IV.1. Star Geometric Configuration

The magnetic induction dispersion and the magnetic induction amplitude at the distance value of $Z = 0$ cm from the primary coils are shown in Fig. 7 and Fig. 8.

The lines, blue, brown and gray represent the values of the magnetic induction measured in (mT).

These lines show the measured values on the circumferences radio value of 100 mm, 200 mm and 300 mm, respectively. The lines yellow and black represent the average of the maximum and minimum values.

The three primary coils were placed in star geometrical configuration and were aligned with the radial lines of 90°, 210° and 330°. It is noted that the three maximums are reached close to these three positions Fig. 8. The Fig. 9 shows the magnetic induction amplitude in the same configuration of the primary coils as used previously, but with the probe in horizontal longitudinal position, shown in Fig. 5. The average of the highest measured values of the magnetic induction is significantly lower than the average calculated from the previous experiments. However, the average of the minimum values now, is slightly higher.

The gap between the average of the maximums values and the minimums values are greatly reduced compared to the values obtained in the previous test conditions.

This can be observed through the gap between the yellow and black lines, in Fig. 9.

Fig. 10 shows the magnetic induction amplitude in the same conditions as the previously but with the probe in horizontal transversal position, as shown in Fig. 6.

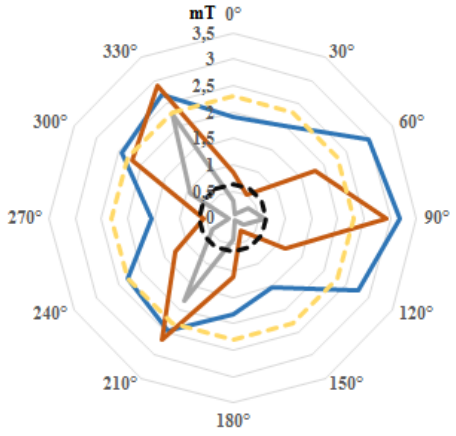

Fig. 7. Probe in vertical position: planar induction dispersion at $Z = 0$ cm

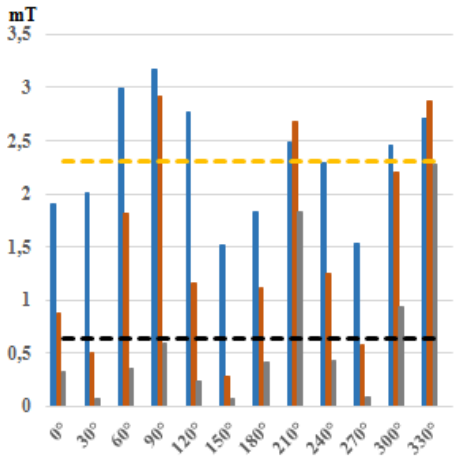

Fig. 8. Probe in vertical position: magnetic induction amplitude at $Z = 0$ cm

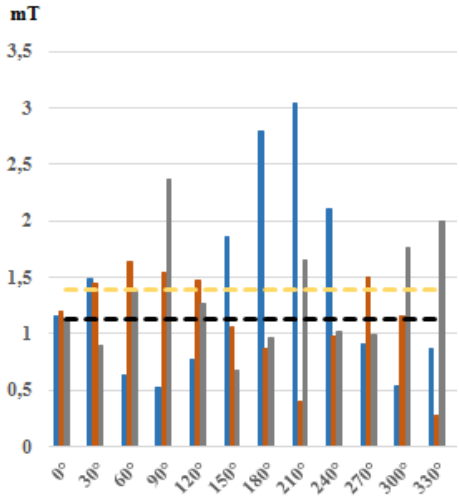

Fig. 9. Probe in horizontal longitudinal position: magnetic induction amplitude at $Z = 0$ cm

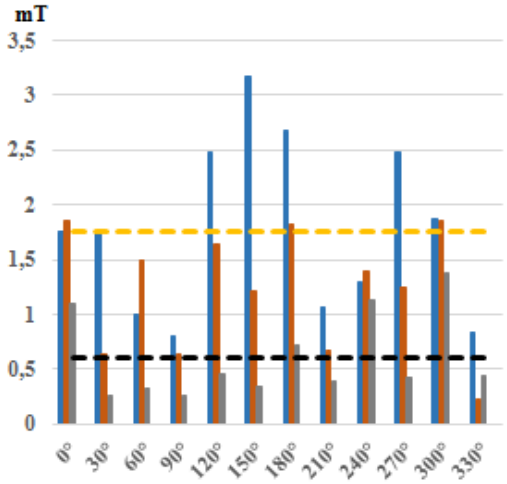

Fig. 10. Probe in horizontal transversal position: magnetic induction amplitude at $Z = 0$ cm

Under the conditions of this configuration, the minimum values are located in places where previously were seen the maximums. The maximum values of the magnetic induction are now located at the intermediate arcs between the positions of the primary coils.

The magnetic induction values measured at a gap (distance) of $Z = 5$ cm between the primary coils and the probe are shown in Fig. 11 to Fig. 13.

The measuring procedures were exactly equal to the previous tests, first with the probe in vertical position, later with the probe in horizontal longitudinal position.

The magnetic induction dispersion and magnetic induction amplitude, obtained at a gap (distance) Z=10 cm between the probe and the primary coils are shown in Fig. 14 to Fig. 17. The tests sequence is the same as the previous.

The magnetic induction amplitude in two different positions is shown in Fig. 16 and Fig. 17. In the first one, the data was obtained with the probe in horizontal longitudinal position and the second the probe was in horizontal transversal position.

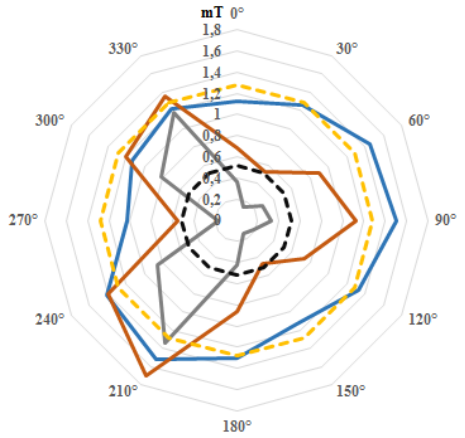

Fig. 11. Probe in vertical position: planar magnetic induction dispersion at Z = 5 cm

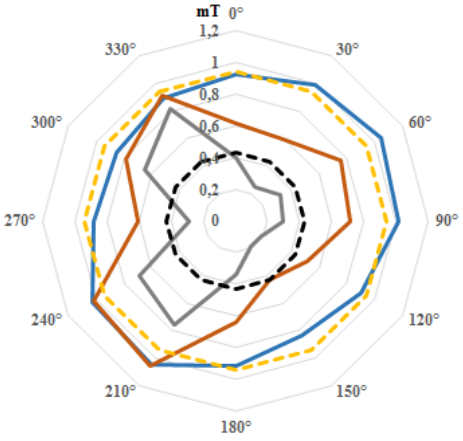

Fig. 14. Probe in vertical position: planar magnetic induction dispersion at Z = 10 cm

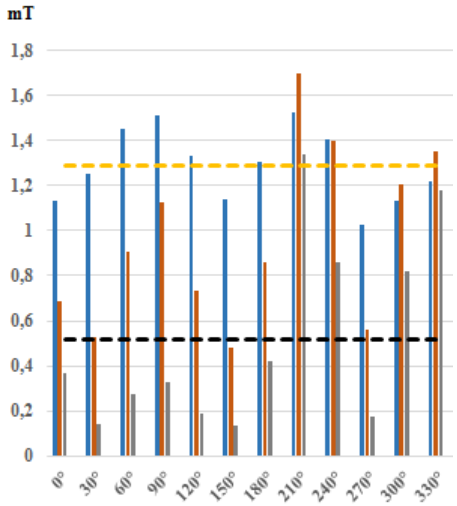

Fig. 12. Probe in vertical position: Magnetic induction amplitude at Z = 5 cm

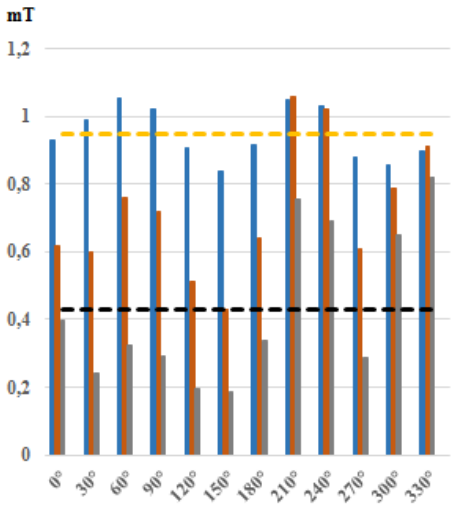

Fig. 15. Probe in vertical position: magnetic induction amplitude at Z = 10 cm

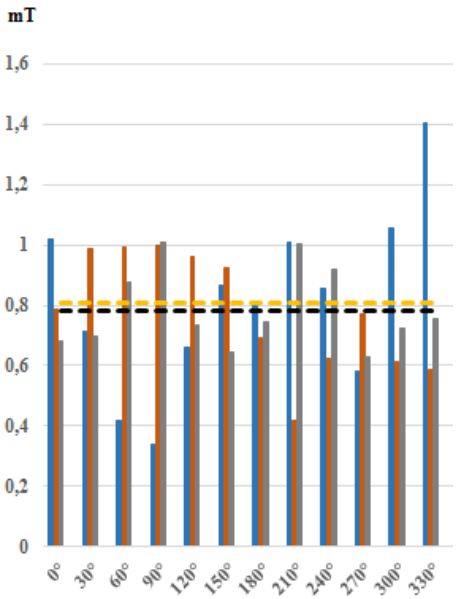

Fig. 13. Probe in horizontal longitudinal position: magnetic induction amplitude at Z = 5 cm

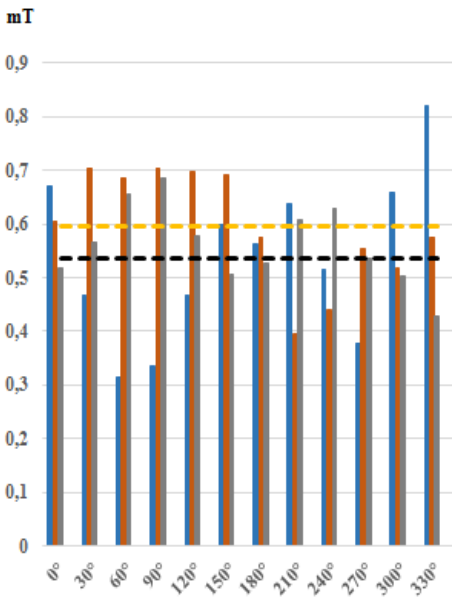

Fig. 16. Probe in horizontal longitudinal position: magnetic induction amplitude at Z = 10 cm

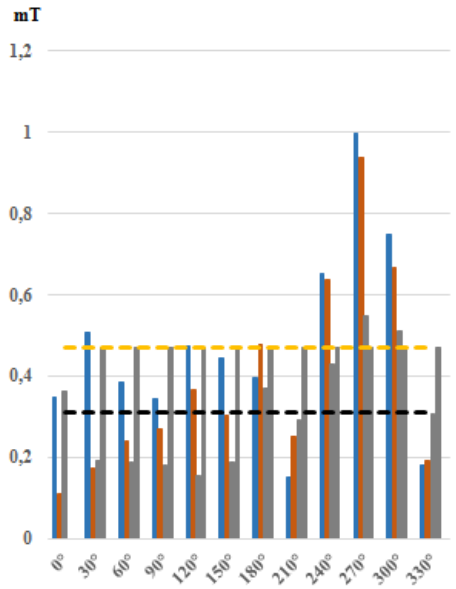

Fig. 17. Probe in horizontal transversal position: magnetic induction amplitude at *Z*=10 cm

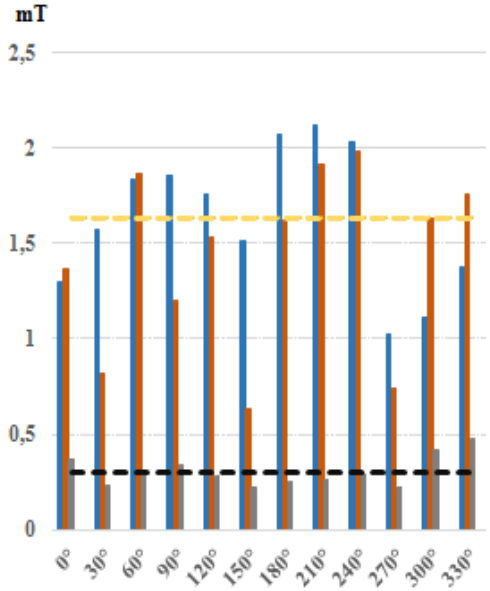

Fig. 19. Probe in vertical position: magnetic induction amplitude at $Z = 0$ cm

IV.2. Delta Geometric Configuration

The magnetic induction values measured on the delta geometric configuration are shown in Fig. 18 to Fig. 29.

The triangle's vertices formed by the three primary coils were placed on radial lines of 90°, 210° and 330°.

The tests sequence was the same as the previous.

First, the probe was placed in vertical position, then in horizontal longitudinal position and finally in horizontal transversal position shown in Fig. 4 to Fig. 6.

The magnetic induction dispersion and magnetic induction amplitude with a gap value of $Z = 0$ cm between the primary coils and the probe are shown in Fig. 18 and Fig. 19. The maximum values of the magnetic induction were obtained around the vertices position, as expected. The grey line represents measured values of the magnetic induction on the outer circumference (larger diameter). These values have naturally, lesser amplitudes.

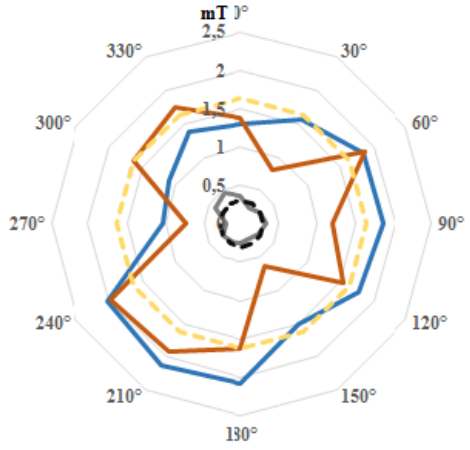

Fig. 18. Probe in vertical position: planar magnetic induction dispersion at *Z*=0 cm

The magnetic induction values obtained at the same conditions as the previous ones, but with the probe in horizontal longitudinal position is shown in Fig. 20.

The gap between the maximum and minimum average is significantly reduced. This is due to the increase of the minimum values of the magnetic induction.

The magnetic induction amplitude with the probe in horizontal transversal position is shown in Fig. 21.

The minimum measured values of the magnetic induction are now found where, in the previous configuration, the maximum values were measured. This is due to the probe position in relation to the magnetic force lines. The gap between the maximum and the minimum values is now higher, due to the reduction of the minimum values.

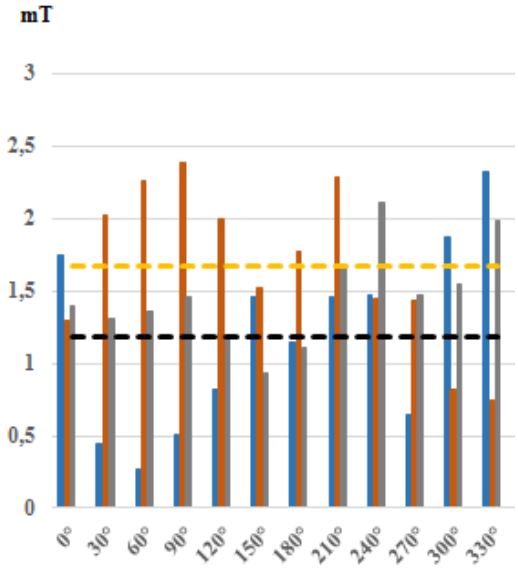

Fig. 20. Probe in horizontal longitudinal position: magnetic induction amplitude at $Z = 0$ cm

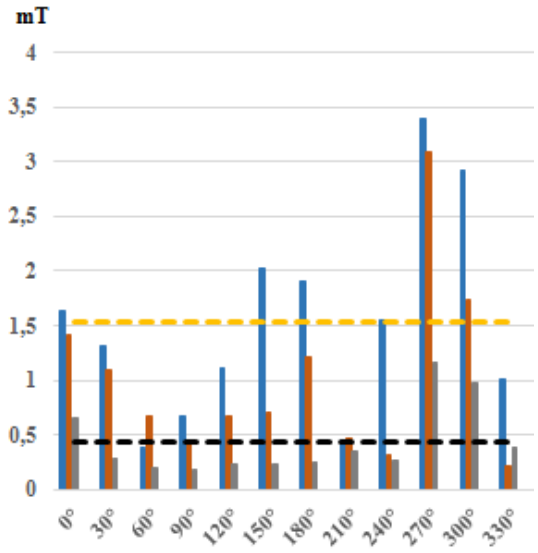

Fig. 21. Probe in horizontal transversal position: magnetic induction amplitude at Z=0 cm

The magnetic induction dispersion and the magnetic induction amplitude at a gap value of 5 cm between the primary coils and the probe in vertical position are shown in Fig. 22 and in Fig. 23. The magnetic induction dispersion shape is close to the obtained with the probe in same position but at $Z = 0$ cm. The magnetic induction amplitude with the probe in horizontal longitudinal position is shown in Fig. 24.

The gap between the maximum average magnetic induction values and the minimum average magnetic induction values is reduced mainly because the maximum value had a significant decrease. The planar magnetic induction dispersion and the magnetic induction amplitude, at a gap of 10 cm between the probe and the primary coils are shown in Fig. 25 to Fig. 29.

The tests were performed in the same sequence as the previous. First, the probe was placed in vertical position, then in horizontal longitudinal position and finally, the probe in horizontal transversal position. The values decrease, as expected, along with the increase of the gap between the primary coils and the probe.

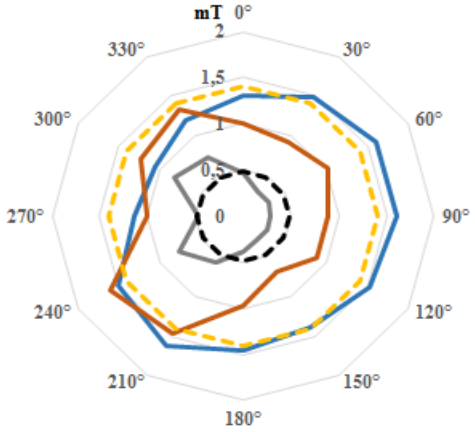

Fig. 22. Probe in vertical position: planar magnetic induction dispersion at $Z = 5$ cm

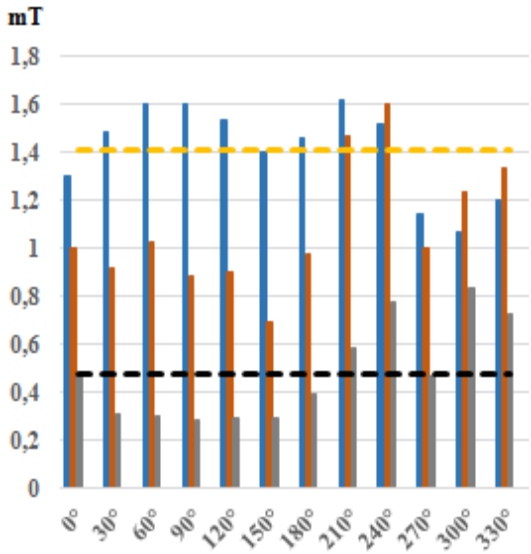

Fig. 23. Probe in vertical position: magnetic induction amplitude at Z=5 cm

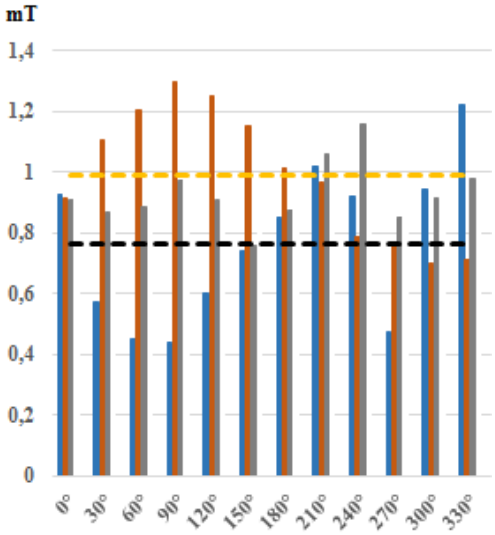

Fig. 24. Probe in horizontal longitudinal position: magnetic induction amplitude at $Z = 5$ cm

Fig. 25 and Fig. 26 show the shape of the intensity of the magnetic induction is more circular although there was a significant drop in the average of the maximum values (yellow line).

Fig. 27 and Fig. 28 show the planar magnetic induction dispersion and the magnetic induction amplitude with the same configuration but with the probe in horizontal longitudinal position.

The maximum average value suffered a slight reduction when compared with the induction value when the probe is in vertical position. This is due to different alignment of the probe related to the magnetic induction line forces. The magnetic induction amplitude measured with the probe in horizontal transversal position is shown in Fig. 29. The values obtained are significantly reduced.

The major cause is, again, the probe alignment with the magnetic force lines.

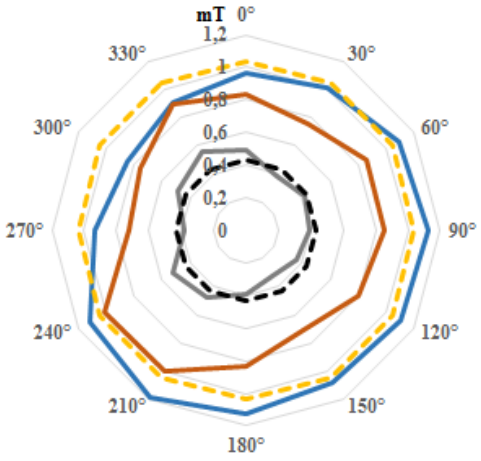

Fig. 25. Probe in vertical position: planar magnetic induction dispersion at *Z*=10 cm

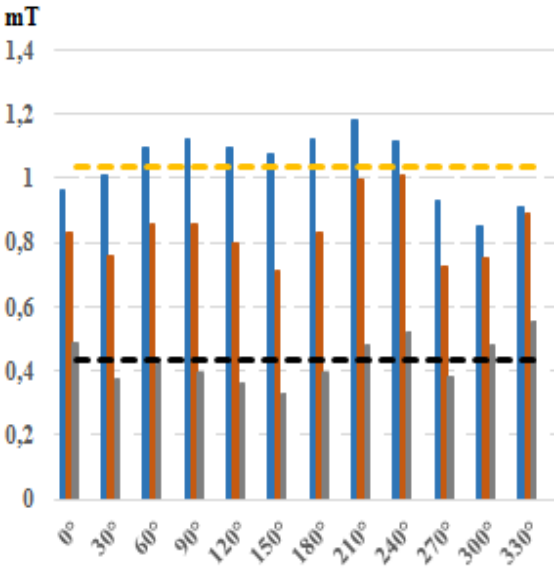

Fig. 26. Probe in vertical position: magnetic induction amplitude at *Z* = 10 cm

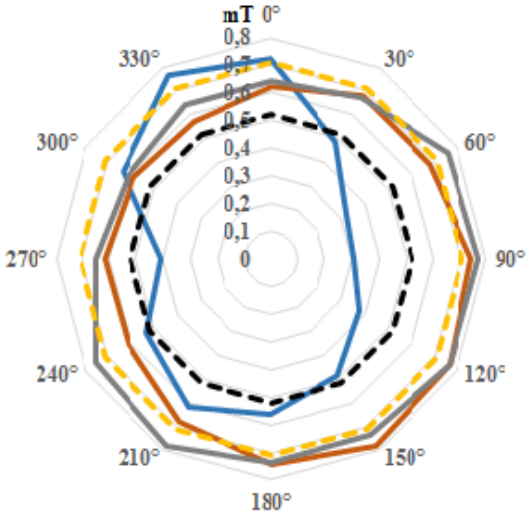

Fig. 27. Probe in horizontal longitudinal position: planar magnetic induction dispersion at Z=10 cm

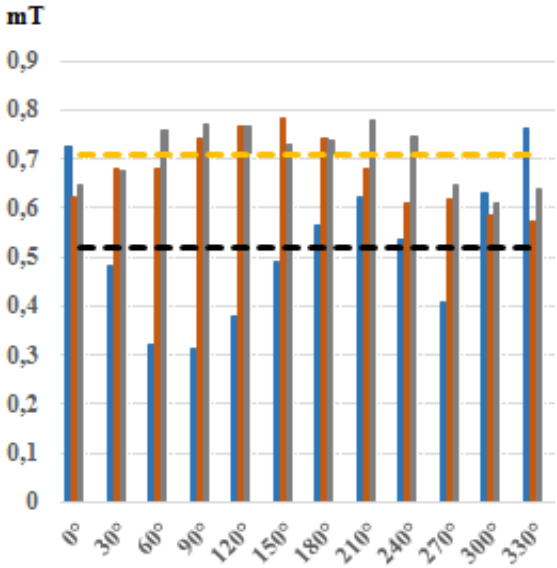

Fig. 28. Probe in horizontal longitudinal position: magnetic induction amplitude at *Z* = 10 cm

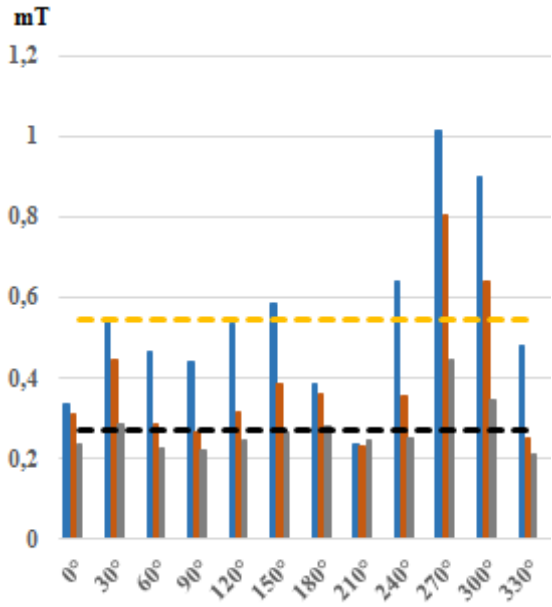

Fig. 29. Probe in horizontal transversal position: magnetic induction amplitude at *Z* = 10 cm

V. Conclusion

The battery charging system using wireless power transfer has a key point: the magnetic circuit must enable the transfer of electrical energy being less sensitive to misalignment. This work was carried out in order to map the magnetic induction of a three-phase system and to clarify the best choice of operation.

The star geometric configuration has the magnetic induction lines concentrated around the star vertex. This is the main reason for the high sensitivity to the misalignment problems making this point very critical.

The delta geometric configuration has the magnetic induction lines more concentrated around the vertices of

the triangle formed by the three primary coils. This allows a better uniform magnetic induction spreading, making the system less sensitive to misalignment.

The delta geometric configuration allows obtaining the magnetic induction distribution almost uniform and circular with a maximum average value of 1 mT, at a gap of 10 cm between the primary coils and the probe.

The delta geometric configuration of the primary coils is proved to be the best. The receiver may contain only one coil finding a good magnetic coupling with any of the three phases at a larger area, where the magnetic induction was discovered to be sufficiently widely and uniformly distributed.

This will be the best choice for transmitting electric power through magnetic induction, as it is necessary in the wireless power transfer system.

References

[1] S. Mohammed, K. Ramasamy, T. Shanmuganantham, Wireless power transmission a next generation power transmission system, *International Journal of Computer Applications*, vol. 1, n. 13, 2010, pp. 100-103.

[2] S. Lukic, Z. Pantic, Cutting the cord – Static and dynamic inductive wireless charging of electric vehicle, *IEEE Electrification Magazine, September*, vol. 1, n. 1, 2013, pp. 57-64.

[3] S.S. Valtchev, E. Baikova, L. Jorge, Electromagnetic field as the wireless transporter of energy, *Facta Universitis*, vol. 25, n. 3, 2012, pp. 171-181.

[4] S- Pawade, T. Nimje, D. Diwasw, Goodby wires: approach of wireless power transmission, *International Journal of Emerging technology and Advance Engineering*, vol. 2, n. 4, 2012, pp. 382-387.

[5] S. Das Gupta, Md.S. Islam, K.Md. Nuronnabi, M.S. Hossain, Md.Z. Hasan, Design & implementation of cost effective wireless power transmission model: good bye cables, *International Journal of Scientific and Research Publications*, vol. 2, n. 12, 2012, pp. 1-9.

[6] D.M. Vilathgamuwa, J.P. Sampath, Wireless power transfer (WPT) for electric vehicles (EVs)-present and future trends, *Plug in Electric Vehicles in Smart Grids*, Springer, 2014, pp. 33-60.

[7] X. Lu, P. Wang, D. Niyato, D.I. Kim, Z. Han, Wireless charging technologies: fundamentals, standards, and network applications, *IEEE Communications Surveys and Tutorials*, vol. 8, n. 2, 2015, pp. 1413-1452.

[8] K. Kusaka, J. Itoh, Reduction of reflected power loss in AC-DC converter for wireless power transfer system, *IEE Journal of Industry Applications*, vol. 2, n. 4, 2013, pp. 195-203.

[9] X. Wei, Z. Wang, H. Dai, A critical review of wireless power transfer via strongly coupled magnetic resonances, *Energies*, vol. 7, n. 7, 2014, pp. 4316-4341.

[10] N. Shinohara, Power without wires, *IEEE Microwave Magazine*, vol. 12, n. 7, 2011, pp. S64-S73.

[11] W.C. Brown, The history of the development of the rectenna, *Proceedings of the Johnson Space Center Workshop on Microwave Power Transmission and Reception*, 1980, pp. 203-212, Houston, USA.

[12] P.E. Glaser, Power from the sun: its future, *Science*, vol. 162, n. 3856, 1968, pp. 857-886.

[13] K. Wu, D. Choudhury, H. Matsumoto, Wireless power transmission, technology and applications, *Proceedings IEEE*, vol. 101, n. 6, 2013, pp. 1271-1275.

[14] N. Shinohara, Y. Kubo, H. Tonomura, Mid-distance wireless power transmission for electric truck via microwaves, *Proceeding of the URSI International Symposium on Electromagnetic Theory, 2013*, pp. 841-843, Hiroshima, Japan.

[15] Z. Harouni, L. Cirio, L. Osman, A. Gharsallah, O. Picon, A dual circularly polarized 2,45-GHz rectenna for wireless power transmission, *IEEE Antennas and Wireless Propagation Letters*, vol. 10, 2011, pp. 306-309.

[16] W. Huang, B. Zhang, X. Chen, K. Huang, C. Liu, Study on an s-band rectenna array for wireless microwave power transmission, *Progress in Electromagnetics Research*, vol. 135, 2013, pp. 747-758.

[17] L. Ke, G. Yan, S. Yan, Z. Wang, D. Liu, Improvement of the coupling factor of litz wire coil pair with ferrite substrate for transcutaneous, *Progress in Electromagnetics Research M*, vol. 39, 2014, pp. 41-52.

[18] S.I. Park, Enhancement of wireless power transmission into biological tissues using a high surface impedance ground plane, *Progress in Electromagnetic Research*, vol. 135, 2013, pp. 123-136.

[19] F. Jolani, J. Mehta, Y. Yu, Z. Chen, Design of wireless power transfer systems magnetic resonance coupling for implantable medical devices, *Progress in Electromagnetic Research Letters*, vol. 40, 2013, pp. 141-151.

[20] E.G. Kiline, G. Conus, C. Weber, B. Kawkabani, F. Maloberti, C. Dehollain, A system for wireless power transfer of micro-system in-vivo implantable in freely moving animals, *IEEE Sensors Journal*, vol. 14, n. 2, 2014, pp. 522-531.

[21] S. Atluri, M. Ghovanloo, Design of a wideband power-efficient inductive wireless link for implantable biomedical devices using multiple carriers, *Proceedings of the 2nd International IEEE EMBS Conference on Neural, 2005*, pp. º533-537.

[22] G.A. Covic, J.T. Boys, M.L.G. Kissin, H.G. Lu, A three-phase inductive power transfer system for railway-powered vehicles, *IEEE transactions on Industrial Electronics, vol. 54, n. 6, 2007*, pp. 3370-3378.

[23] R. Bosshard, U. Badstübner, J. W. Kolar, I. Stevanović, Comparative Evaluation of Control Methods for Inductive Power Transfer, *Proceedings of the International Conference on Renewble Energy Research and Applications*, pp. 1-6, Nagasaki, Japan, 2012.

[24] K. Hwang, S. Kim, S. Kim, Y. Chan, S. Ahn, Design of wireless power transfer system for railway application, *International Journal of Railway*, vol. 5, n. 4, 2012, pp. 167-174.

[25] International Electrotechnical Commission (IEC), visited in July 8th, 2016, (http://www.iec.ch).

[26] International Organization for Standardization (ISO), visited in July 7th, 2016, (http://www.iso.org).

[27] European Committee for Electrotechnical Standardization (CENELEC), visited in July 7th, 2016, (http://www.cencenelec.eu).

[28] P.G. Pereirinha, J.P. Trovão, Multiple energy sources hybridization: the future of electric vehicles?, *New Generation of Electric Vehicles, 2012*, Intech.

[29] J. Douglas, Electromagnetic fields and human health, *Electr. Power Res. Inst. J.*, vol. 9, n. 4, 1984, pp. 14-21.

[30] K.H. Mild, M. Sandström, Guide electromagnetic fields in working life a guide to risk assessment, *European Trade Union Institute, 2015*, Brussels, Belgium.

[31] L.F. Romba, S.S. Valtchev, R. Melício, Three-phase magnetic field system for wireless energy transfer, *Proceedings of the International Symposium on Power Electronics, Electrical Drives and Motion, 2016*, pp. 73-78, Capri, Italy.

[32] L.F. Romba, S.S. Valtchev, R. Melício, Improving magnetic coupling for battery charging through 3D magnetic flux, *Proceedings of the IEEE 17th International Conference on Power Electronics and Motion Control, 2016*, pp. 291-297, Varna, Bulgaria.

[33] L.F. Romba, Stanimir S. Valtchev, R. Melício, Wireless energy transfer with three-phase magnetic field system: experimental results, *Proceedings of the International Conference on Renewable Energies and Power Quality, 2016*, pp. 1-5, Madrid, Spain.

[34] Baikova, E., Valtchev, S., Melicio, R., Krusteva, A., Pires, V., Study of the Electromagnetic Interference Generated by Wireless Power Transfer Systems, (2016) *International Review of Electrical Engineering (IREE)*, 11 (5), pp. 526-534.

[35] Shadmehr, H., Grimaccia, F., Gruosso, G., Mussetta, M., Zich, R., Optimized Antenna for Low UHF Range Wireless Power Transfer, (2013) *International Journal on Communications*

Antenna and Propagation (IRECAP), 3 (1), pp. 21-26.

[36] Bindu, G., Ramachandran, H., General Public Exposure Radiation Measurements in the Vicinity of a Wireless Power Transfer Prototype System, (2013) *International Journal on Communications Antenna and Propagation (IRECAP)*, 3 (3), pp. 169-175.

Authors' information

[1]UNINOVA/CTS, Faculdade de Ciências e Tecnologia, Universidade Nova de Lisboa, Portugal.

[2]IDMEC, Instituto Superior Técnico, Universidade de Lisboa, Portugal.

[3]Departamento de Física, Escola de Ciências e Tecnologia, Universidade de Évora, Portugal.

Luis R. Jorge, received the BSc in Electronics and Telecommunications and the degree in Electrical Power Distribution and Power Control Systems from Instituto Superior de Engenharia, Lisbon, Portugal. He received the MSc by Faculdade de Ciencias e Tecnologia (FCT), Universidade Nova de Lisboa (UNL), Portugal in Renewable Energy and Sustainable Energy Systems. He is currently pursuing the Ph.D. degree at UNL. His professional carrier was developed to a great extend in radar, navigation, communications, and support equipment engineering. He is now a researcher at the research center CTS-UNINOVA of FCT/UNL with a special interest in the wireless power transfer for electric vehicles, applying electromagnetic resonant coupling and magnetic core reactor.

Stanimir S. Valtchev (IEEE: M'93, SM'08) Professor Auxiliar of Power Electronics, Department of Electrical Engineering of the Faculty of Science and Technology, Universidade Nova de Lisboa, Portugal. Best graduate (MSc) of 1974, Technical University Sofia (TUS), in semiconductor and electronics technology, military service in radars, researcher in medical equipment and power converters and laser supplies, Auxiliary Director of the Centre of Robotics of TUS. In 1987 worked in TU Delft as Assistant Professor, since 1988 Assistant Professor in TUS (Power Supplies and Converters), Deputy Dean of TUS. Working on HF resonant power converters, IEEE Meritorious Paper Award, 1997, Best Paper Award from PEMC2014. Since 1994, teaching and consulting in Portugal and in the Netherlands. Based on a versatile experience, the research includes energy conversion, energy harvesting, wireless energy transfer, electric vehicles, energy management and storage, smart grids, tunnel FET devices and biosensors. He was the General Chair of the IEEE-PEMC2016 conference and since 2012 he is Invited Full Professor of Burgas Free University, Bulgaria.

R. Melício, was born in Lisbon, Portugal, and received the MSc in 2004, from Instituto Superior Técnico, Lisbon, Portugal, received the PhD in 2010 from Universidade da Beira Interior, Portugal, received the Post-PhD in 2012 from Fundação para a Ciência e a Tecnologia, Lisbon, Portugal and Habilitation in 2014 from the Universidade de Évora, Portugal. He is member of IDMEC research laboratory and an Assistant Professor with Habilitation at Universidade de Évora. He has worked more the 20 years in the electrical and oil industries. His research interests include: power electronics and its applications; power systems management and operation; renewable energies; smart grids. He is a senior member of the IEEE Industrial Electronics Society.

